Journal of Alloys and Compounds 502 (2010) 310–318

Contents lists available at ScienceDirect

Journal of Alloys and Compounds

journal homepage: www.elsevier.com/locate/jallcom

Microstructure and room temperature mechanical properties of hot-pressed Nb–Si–Ti–Fe alloys

X.L. Wang[a,*], G. Wang[b], K.F. Zhang[a]

[a] National Key Laboratory for Precision Heat Processing of Metal, Harbin Institute of Technology, Harbin 150001, PR China
[b] School of Materials Science and Engineering, Harbin Institute of Technology at Weihai, Weihai 264209, PR China

ARTICLE INFO

Article history:
Received 14 December 2009
Received in revised form 23 April 2010
Accepted 28 April 2010
Available online 5 May 2010

Keywords:
Nb-based alloy
Ball milling
Hot pressing
Microstructure
Fracture toughness

ABSTRACT

Bulk alloys were fabricated by uniaxial hot pressing from ball milled Nb-Si–Ti–Fe powder mixtures with the fixed Si content (16 at.%) and various compositions of Ti and Fe, and the effects of Ti and/or Fe on the ball milling, microstructure and room temperature mechanical properties of the materials were investigated. It was revealed that the Ti addition inhibited the ball milling process with the same milling parameters. For the hot-pressed alloys, Nb_4FeSi phase was detected in the alloys containing Fe, and Fe mainly dissolved into niobium silicides from the result of elemental mapping. The solubility of Si in Nbss was enhanced by the addition of Ti, and Nb_3Si expected was not observed in the Ti-bearing alloys that may be due to the lower Ti content in the reaction zone between the particles. The Ti-added alloys hot pressed from a shorter time showed the coarser microstructure with Nbss in the shape of narrow strip distributed in river pattern, while near-equiaxed macrostructure was obtained in the Nb–Si–Fe alloys. The improvement in both room temperature fracture toughness and flexural strength was achieved in Ti-added alloys. The toughening and strengthening mechanisms were discussed from the ductile-phase toughening of crack bridging and solid solution strengthening, respectively.

1. Introduction

Because of their high melting point, low density and excellent specific mechanical properties at high temperatures [1–3], niobium–silicide based alloys have been studied as potential candidate for the development of high temperature structural material [4–6], whose operating temperature exceeds that of conventional nickel-based superalloy. However, the intrinsic brittleness of niobium silicides with the limited fracture toughness as low as 3 $MPa^{1/2}$ at ambient temperature [7] inhibits the practical applications of niobium–silicide based alloys. However, it has been demonstrated that the room temperature fracture resistance is improved by incorporating ductile particle reinforcement of Nbss to brittle niobium silicides [8–11]. Moreover, it is well known that the volume fraction, geometry and distribution of ductile phases have significant impact upon the toughness of ductile-phase-toughened materials [12,13]. The toughness improvement through microstructure control has been investigated for the as-cast Nb–Si alloys [14,15], and it has been found that the development of a duplex microstructure, where coarse Nb particles coexist with Nb/Nb_5Si_3 lamellae, provides some compressive ductility at room temperature [15]. At the same time, the crack bridging toughening by a larger sized ductile phase operate effectively in the materials with columnar ductile phase [16–18], and provide the samples with a higher toughness increment via the crack bridging mechanism [19]. Recent studies have involved into the effect of alloying elements such as Ti, Cr, Al, Mo, Fe and B, etc. on the microstructure, mechanical properties and oxidation resistance of multi-component arc-melted Nb–Si alloys [4,20–24]. And few reports have also exhibited the microstructure and/or mechanical characterization of Nb–Si alloys from Nb–Si–Ti ternary system fabricated by unidirectional solidification and reactive hot-pressing sintering [9,25,26]. The Ti addition to the Nb–Si alloys especially improves both room temperature toughness and oxidation resistance, and a recent study [27] has demonstrated that hot extrusion of multiphase Nb–Si–Fe in situ composite also improves the room temperature fracture toughness. As for the processing techniques, casting methods including electron beam melting, vacuum arc melting and directional solidification [4,6,9] are the main ones to prepare Nb–silicide-based composites. To date, the reports on the microstructure and mechanical properties of mechanically alloyed and hot-pressed Nb–Si alloys with the addition of Ti and/or Fe are still poor.

In the present study, bulk Nb–Si alloys with several compositions of Ti and Fe were fabricated by mechanical alloying followed by hot pressing. The aim of this work was to investigate the

* Corresponding author. Tel.: +86 451 86413681; fax: +86 451 86413911.
E-mail address: meng328@163.com (X.L. Wang).

0925-8388/$ – see front matter © 2010 Elsevier B.V. All rights reserved.
doi:10.1016/j.jallcom.2010.04.208

influence of ball milling on the microstructure, and the effect of microstructural control on the room temperature fracture toughness and flexural strength of the hot-pressed Nb–Si materials containing Ti and/or Fe.

2. Experimental procedures

The composition of the investigated alloys is Nb–16 at.%Si–*x* at.%Ti–*y* at.%Fe (*x* = 0, 10, and 18; *y* = 0, 1, and 3). Element powders of Nb (99.5%, 150 μm), Si (99.9%, 60 μm), Ti (99%, 25 μm) and Fe (99.9%, 5 μm) were used as starting materials. Ball milling was carried out at room temperature in a planetary ball mill with stainless steel vials and bearing steel balls under argon atmosphere. The ball-to-powder weight ratio was maintained at 12:1, and the rotation speed employed was 250 rpm. The compound powders milled for 18 and 30 h (the total milling time) were respectively placed into the BN-coated graphite die and hot pressed uniaxially at 1500 °C for 60 min under 30 MPa in argon atmosphere followed by furnace cooling.

The particle morphologies and fracture surfaces of bulk samples were examined by scanning electron microscopy (SEM), while the microstructures and crack propagation of hot-pressed alloys were detected by using backscattered electron (BSE) images. X-ray diffraction (XRD) was performed on the bulk samples to identify the constituent phases, and the experiments were conducted at room temperature with a D/max-rB X-ray diffractometer using Cu Kα radiation (λ = 0.15418 nm). The chemical compositions of the phases were analyzed by using the energy dispersive X-ray spectroscopy (EDX). Flexural strength test was conducted by three-point bending (TPB) specimens with 30 mm span length (total length = 36 mm), 4 mm width and 3 mm thickness in Instron-1186. Facture toughness was evaluated by single edge notch bending (SENB) specimens with 16 mm span length (total length = 20 mm), 4 mm width and 2 mm thickness, but without the introduction of an initial fatigue crack. A straight notch of about 2 mm depth was inserted into each specimen at mid-length using electro-discharge machining (EDM) with 0.1 mm diameter wire.

3. Results and discussion

3.1. Morphologies of milled powder mixtures

The shape and size of Nb–16Si–3Fe and Nb–16Si–18Ti–3Fe powder mixtures after 18 and 30 h milling were observed by SEM, and the micrographs are presented in Fig. 1. There existed quite distinct features of morphology changes for the two milled powder mixtures. In the case of Nb–16Si–3Fe powders, the size of powder particles was reduced significantly after 18 h milling, and the particles showed more uniform distribution and smaller size after 30 h milling. With respect to Nb–16Si–18Ti–3Fe milled powders, plate-like coarse particles with a broad range of size were observed after 18 h milling, and the particle size of 30 h milled powders decreased greatly. However, the powders were still coarser than 18 h milled Nb–16Si–3Fe ones, indicating that the addition of ductile titanium powders retarded the ball milling process. In the case of the same weight, the volume of Nb–16Si–3Fe powder mixtures with Ti is higher since the density of Ti is lower than Nb. Therefore, with the same milling parameters, the ball milling of Nb–16Si–18Ti–3Fe particles developed slower compared to Nb–16Si–3Fe powders.

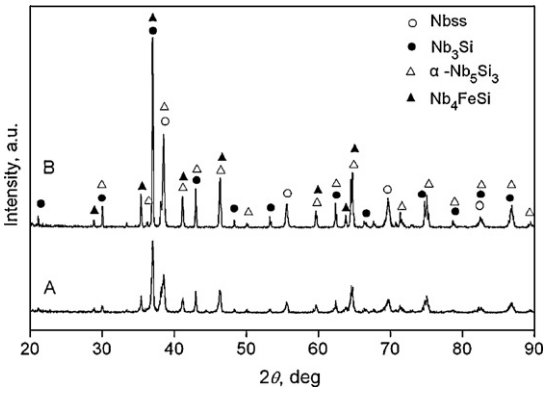

Fig. 2. XRD patterns of Nb–16Si–3Fe alloys made form 18 h (A) and 30 h (B) milled powders.

3.2. Phase composition and microstructures of hot-pressed alloys

The XRD patterns of bulk alloys made from Nb–16Si–3Fe powder mixtures are shown in Fig. 2. Typical peaks of Nbss, Nb_3Si, α-Nb_5Si_3 and Nb_4FeSi were detected in hot-pressed Nb–16Si–3Fe alloys. Si was not identified in the resolution of the X-ray diffractometer, indicating that a complete reaction occurred. Fig. 3 shows

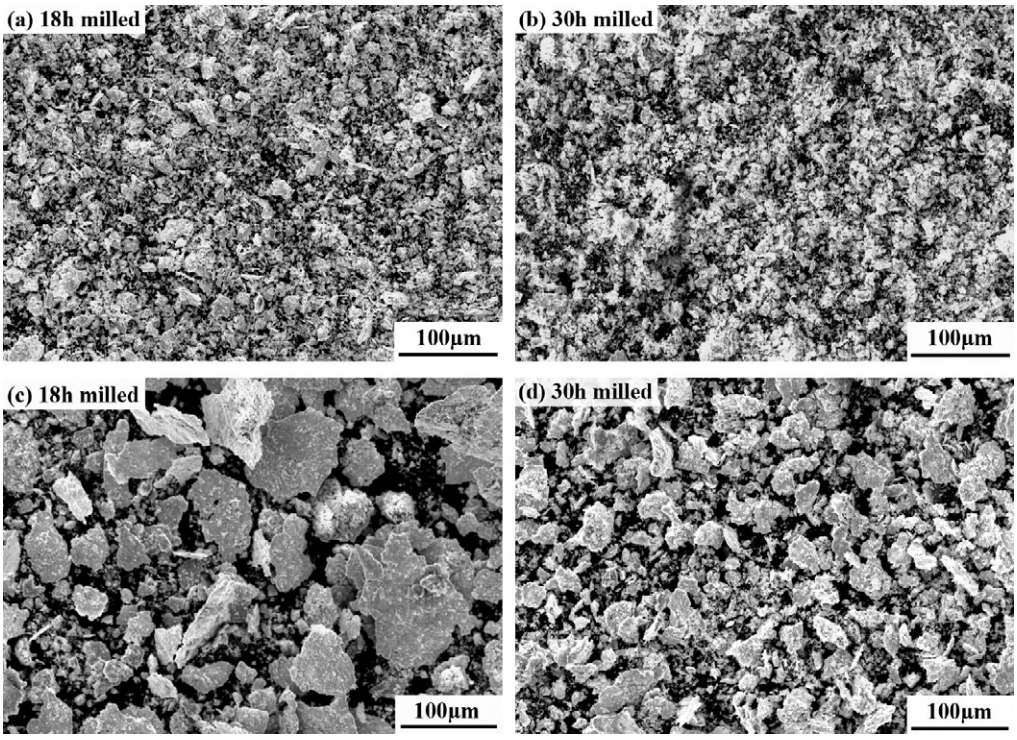

Fig. 1. SEM micrographs of the powder mixtures after 18 and 30 h milling: (a) and (b) for Nb–16Si–3Fe; (c) and (d) for Nb–16Si–18Ti–3Fe.

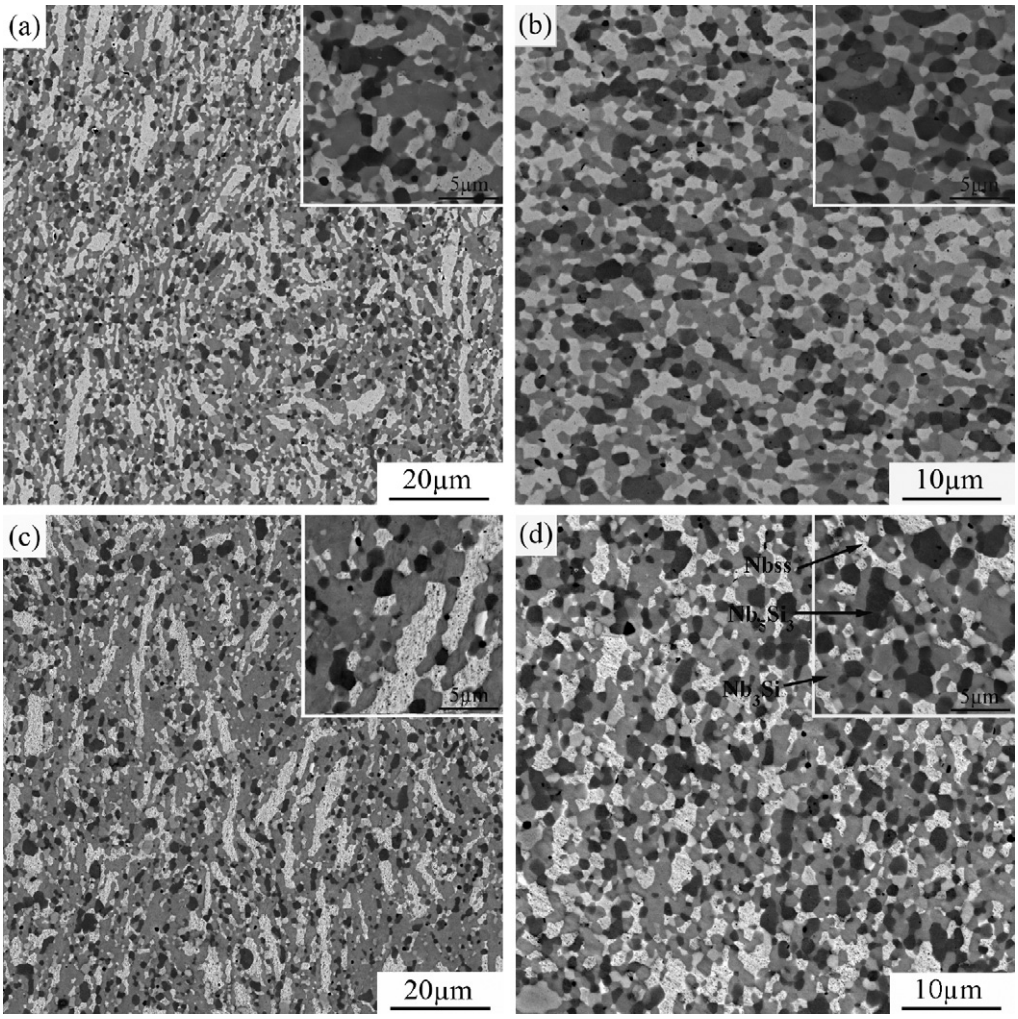

Fig. 3. Backscattered electron images of bulk Nb–Si–Fe alloys consolidated form 18 h (a and c) and 30 h (b and d) milled powders: (a) and (b) for Nb–16Si–Fe; (c) and (d) for Nb–16Si–3Fe. Insets are higher magnification images.

the backscattered electron images of Nb–16Si–Fe and Nb–16Si–3Fe alloys. Nbss phase with the shape of rough banding was observed in alloys consolidated from 18 h milled powders, and intermetallic compounds distributed along the coarse bright phase suggesting that reaction in situ took place at the junction of Nb particles. Comparatively, the microstructures of materials made from 30 h milled powders were much finer, and the constituent phases displayed near-equiaxed shape. Furthermore, the volume fraction of intermetallic compounds was higher than that of alloys made from 18 h milled powders, and it indicates that the enhanced atomic diffusion among different elements was obtained after the longer time milling and accordingly contributed to the formation of intermetallics.

The XRD patterns of hot-pressed alloys consolidated from Nb–16Si–18Ti and Nb–16Si–18Ti–3Fe powder mixtures are shown in Fig. 4, respectively. Nbss, Tiss and α-Nb_5Si_3 phases were detected in both alloys. Besides the above three phases, the peak of ternary phase Nb_4FeSi was also found in the pattern of Nb–16Si–18Ti–3Fe alloy due to the addition of Fe. Figs. 5 and 6 show the backscattered electron images of hot-pressed Nb–16Si alloys with various contents of Ti and Fe from powder mixtures milled for 18 and 30 h, respectively. The white, gray and dark phases corresponded to Nbss, Nb_5Si_3 and Tiss, respectively. Unfortunately, from the figures of this study, it was hard to distinguish the ternary phase Nb_4FeSi only according to a difference in contrast under backscatter imaging conditions. EDX analysis was conducted on the investigated alloys to determine the atomic composition of constituent phases, and element mapping was carried out on Nb–16Si–18Ti–3Fe alloy made from 30 h milled powders to understand the distribution of elements, especially for iron. The results are respectively shown in Table 1 and Fig. 7. Fe was found to mainly distribute in the zone of niobium silicides, and it could be accordingly deduced that the ternary phase with Fe coexisted with the silicides. In addition, for hot-pressed Ti-added alloys, the Ti concentration in Nbss increased with its initial nominal composition increasing and Nbss contains a little higher Si compared to materials without Ti. Furthermore, it was noticeable that Nb_3Si phase was not detected in hot-pressed Nb–Si alloys with Ti and it was not in agreement with the results of as-cast alloys available in the associated literatures [23,24,28]. In those reports, it was demonstrated that high mounts of Ti enhanced the stabilization of Nb_3Si. Nevertheless, a previous investigation by Bewlay et al. [25] on the directionally solidified Nb–Si–Ti ternary alloys with low Ti concentration, i.e. Nb–3Ti–16Si and Nb–9Ti–16Si alloys, demonstrated that they characterized by two-phase microstructure of Nbss and Nb_5Si_3 containing Ti. As seen from the microstructures of Ti-bearing alloys (shown in Figs. 5 and 6), silicides lay along Nbss and/or Tiss, and it was similar with that of hot-pressed Nb–Si–Fe alloys. In view of the above-mentioned data, it was speculated that the solubility of Ti at the adjacent areas of Nb and/or Ti was much lower than the nominal composition used in starting materials. During milling, the atoms of one constituent element were forced to dissolve into the lattice

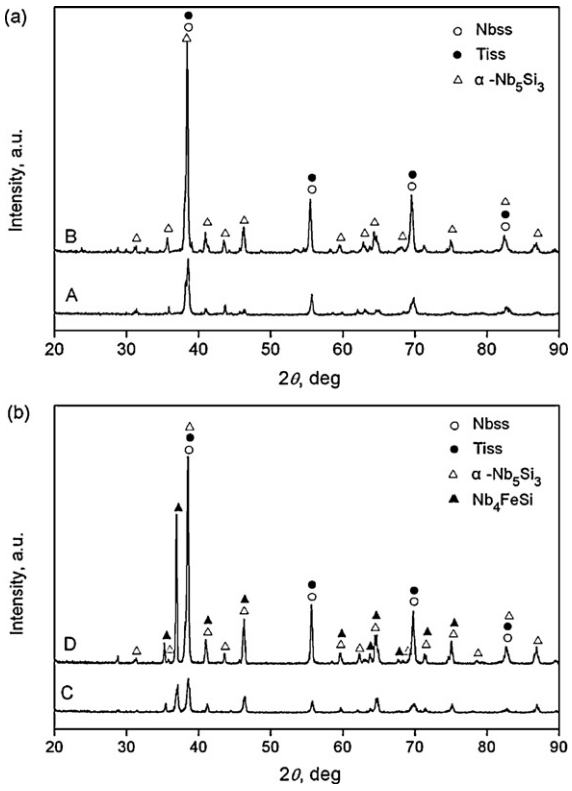

Fig. 4. XRD patterns of bulk alloys of (a) Nb–16Si–18Ti and (b) Nb–16Si–18Ti–3Fe consolidated form 18 h (A and C) and 30 h (B and D) milled powders.

of another component, and the dissolving capacity was related to the concrete milling parameters. As a result, it was possible that the low level of Ti concentration was obtained at the in situ reaction zone of the investigated material in this study, so that the phase composition without Nb_3Si was obtained in the hot-pressed Nb–Si alloys with high amounts of Ti.

In Ti-containing alloys from powder mixtures milled for 18 h, Nbss in the shape of narrow strip distributed in river pattern, and especially, some Nbss phases with severe bending shape were observed. It implies that Nbss retained the morphology of powder particles (Fig. 1 (c)) that the alloys were hot pressed from. In the similar way, some dark Tiss in finer banding also existed in the materials indicating that not all Ti dissolved during milling and participated in the synthesis reaction in hot-pressing process. Furthermore, silicides tended to distribute along the Nbss boundaries and separated Nbss and Tiss. It might be attributed to that the cracked Si embedded in the surface of plastic Nb and Ti particles during milling, and silicides accordingly formed by way of in situ synthesis at the places near to Nb and/or Ti. As for the alloys consolidated from 30 h milled powders, the microstructure was significantly refined and discontinuous Nbss phases were developed. Though some strips of Nbss still existed, both the length and thickness were greatly decreased. After 30 h milling, Nb particles were cracked due to work-hardening (Fig. 1(d)) and Si embedded in the finer Nb particles, so that Nbss phases were cut off by silicides synthesized in the hot-pressing process. Furthermore, some rough Tiss shared the similar dimension with Nbss of alloys made from powders of the longer milling time, suggesting that particle size of Ti reduced slower in comparison with that of Nb at the later period of ball milling under the given condition in this study.

In addition, as shown in Figs. 5 and 6, the banding Nbss in the alloys with 10 at.% Ti was much narrower than that in the corresponding alloys of Nb–16Si–18Ti system under the same preparation condition. It implies that more Ti additions kept down the milling process and it was consistent with the results shown in Fig. 1. Moreover, it was noted that, for the alloys with the equal amount of Ti, the microstructure became finer and the volume fraction of intermetallic compounds increased when the content of Fe increased to 3 at.%. It was especially evident for Nb–16Si–10Ti system suggesting that the addition of Fe might promote the evolution of ball milling.

3.3. Mechanical properties of the hot-pressed alloys

The results of flexural strength and fracture toughness for the investigated alloys at room temperature are summarized in Table 2. Hot-pressed Nb–Si alloys with only Fe addition exhibited the lower flexural strength in comparison with Ti-added alloys. In addition, in alloys with a fixed content of Ti, flexural strength showed the descending trend with increasing Fe to 3 at.%, and there existed no marked difference in values of flexural strength between the alloys from 18 and 30 h milled powders. Interestingly, it is obvious that the volume fraction of silicides did not definitively affect the flexural strength of the investigated alloys. It was inconsistent with the results obtained by Sha et al. [29], that an increase in the volume fraction of Nb_5Si_3 phase improved the high temperature strength of the Nb–Nb_5Si_3 in situ composites, as niobium silicides mainly supply the strength. Li and Peng [26] also reported the opposite

Table 1
Compositions of the phases of Nb–16Si alloys with various Ti and Fe content determined by EDX analysis.

Sample	Phase	Composition (at.%) (18 h/30 h)			
		Nb	Si	Ti	Fe
Nb–16Si–3Fe	Nbss	99.08/98.79	0.92/1.21	–	–
	Nb_5Si_3	65.16/60.50	31.06/35.41	–	3.78/4.09
	Nb_3Si	73.4/74.12	24.5/23.05	–	2.1/2.83
Nb–16Si–10Ti	Nbss	95.05/94.55	1.43/1.81	3.52/3.04	–
	Nb_5Si_3	64.34/63.47	30.33/32.22	5.34/4.32	–
	Tiss	7.42/12.92	1.92/3.76	90.66/83.32	–
Nb–16Si–10Ti–3Fe	Nbss	94.92/95.15	1.32/1.59	3.76/3.26	–
	Nb_5Si_3	63.59/60.00	30.48/31.23	6.07/4.88	3.77/3.90
	Tiss	10.94/15.52	3.80/5.00	85.26/79.48	–
Nb–16Si–18Ti	Nbss	93.40/92.83	1.84/2.96	4.76/4.21	–
	Nb_5Si_3	61.85/64.32	29.69/30.50	9.47/5.18	–
	Tiss	5.64/9.73	2.18/3.66	92.18/86.62	–
Nb–16Si–18Ti–3Fe	Nbss	92.51/93.26	1.64/1.88	5.85/4.85	–
	Nb_5Si_3	56.56/59.44	29.81/30.27	9.74/6.26	3.89/4.03
	Tiss	11.68/20.23	2.87/4.23	85.45/75.53	–

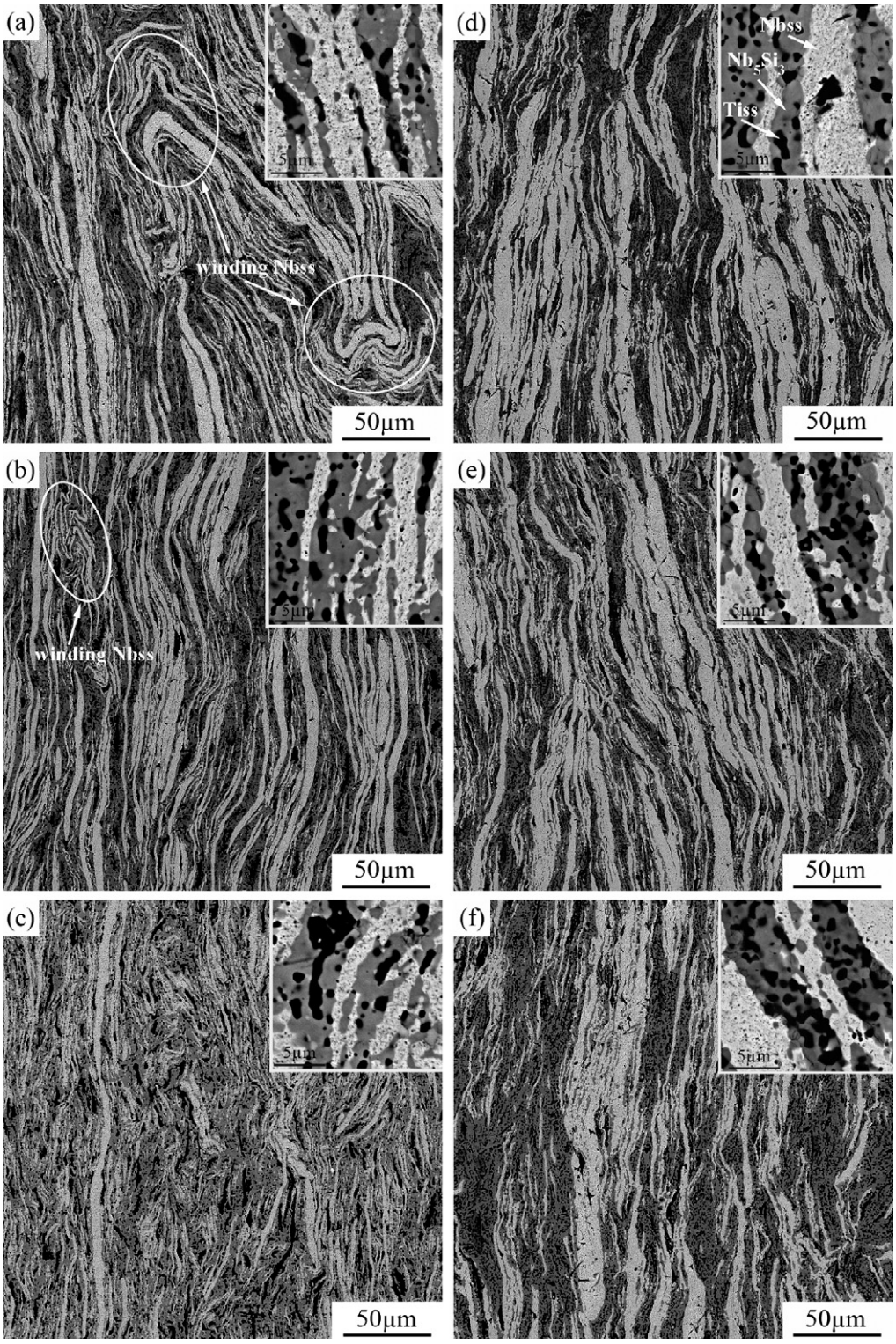

Fig. 5. Backscattered electron images of bulk alloys hot pressed from powder mixtures milled for 18 h: (a) Nb–16Si–10Ti, (b) Nb–16Si–10Ti–Fe, (c) Nb–16Si–10Ti–3Fe, (d) Nb–16Si–18Ti, (e) Nb–16Si–18Ti–Fe and (f) Nb–16Si–18Ti–3Fe. Insets are higher magnification images.

tendency that the flexural strength reduced with the content of niobium silicides enhancing, and they attributed it to residual pores located at the boundaries in the samples with a higher content of niobium silicides. However, the residual pores in the alloys of this study were not as critical as those observed in the literature and it implies that strengthening mechanism other than the enhancement effect of reinforced phase (niobium silicide) contributed to the present result. In addition, Ti-bearing alloys exhibited the higher flexural strength, and the content of Ti dissolving into Nb increased with its composition in the original alloys increasing. This indicates that solid solution strengthening of Nbss played a significant role in reinforcing the materials. Therefore, the flexural strength of hot-pressed Ti-added alloys enhanced with the volume fraction of Nbss increasing, and was affected less by the reduced

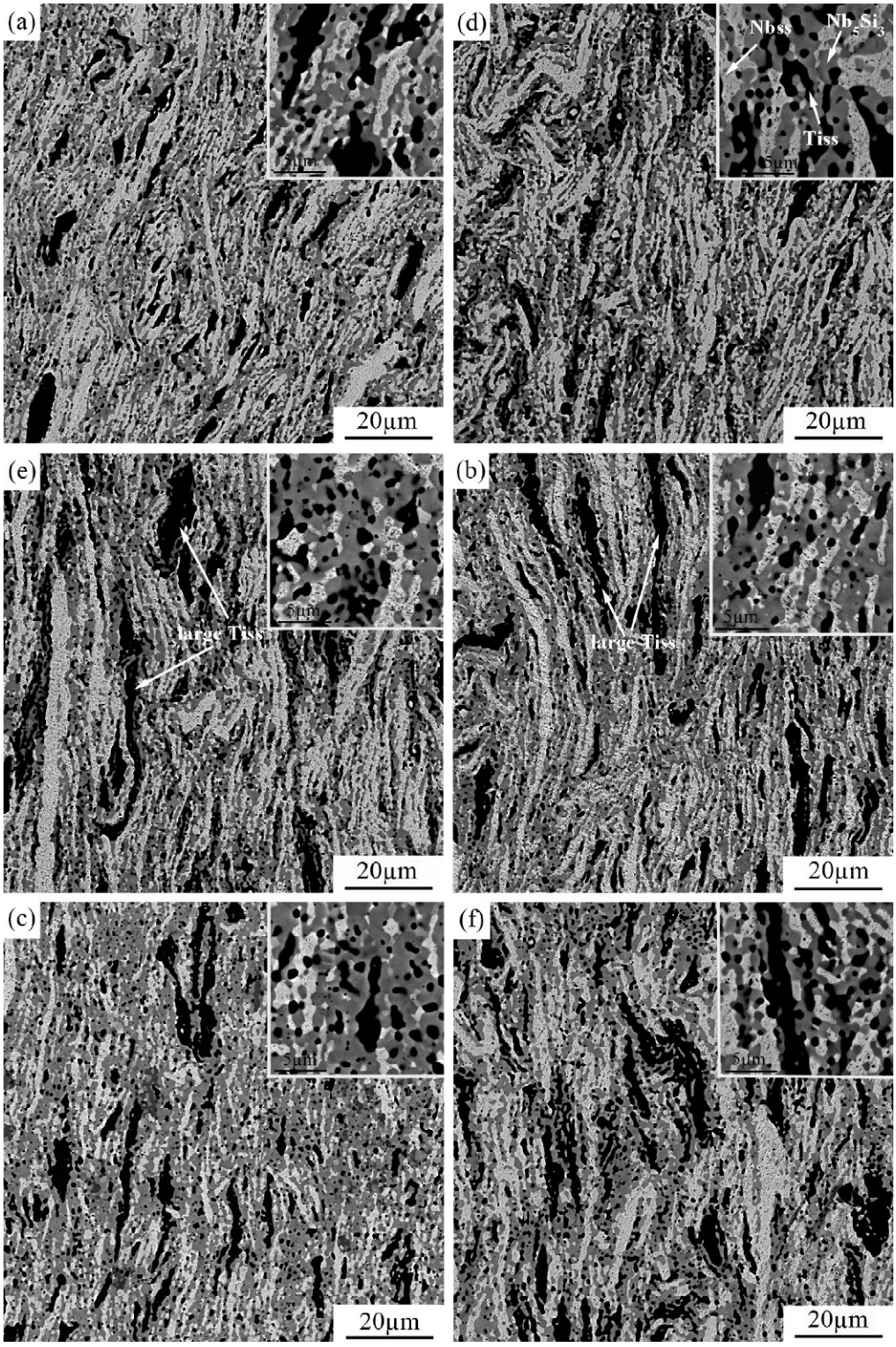

Fig. 6. Backscattered electron images of bulk alloys hot pressed from powder mixtures milled for 30 h: (a) Nb–16Si–10Ti, (b) Nb–16Si–10Ti–Fe, (c) Nb–16Si–10Ti–3Fe, (d) Nb–16Si–18Ti, (e) Nb–16Si–18Ti–Fe and (f) Nb–16Si–18Ti–3Fe. Insets are higher magnification images.

content of niobium silicide. Nevertheless, it can not be concluded that niobium silicide was out of contributing to the strength in this work. From the values in Table 2, it is easily detected that, compared to alloys from 18 h milled powders, samples from 30 h milled powders displayed a little higher flexural strength though they owned less niobium solid solution. It indicates that niobium silicide also offered the strength of alloys from the longer milling time. Furthermore, the addition of Ti was noted to significantly enhance the fracture toughness of the investigated alloys and the hot-pressed Nb–16Si–18Ti alloy from 18 h milled powders exhibited the highest value of fracture toughness over 16 $MPa^{1/2}$. By theoretical calculation, Chan has demonstrated that appropriate Ti could impart fracture toughness resistance in Nb solid solution and Nb-based silicides by altering the crystal structure to promote slip by partial dislocations, reducing the Peierls–Nabarro energy and lowering the anti-phase or complex stacking fault energy [30,31]. How-

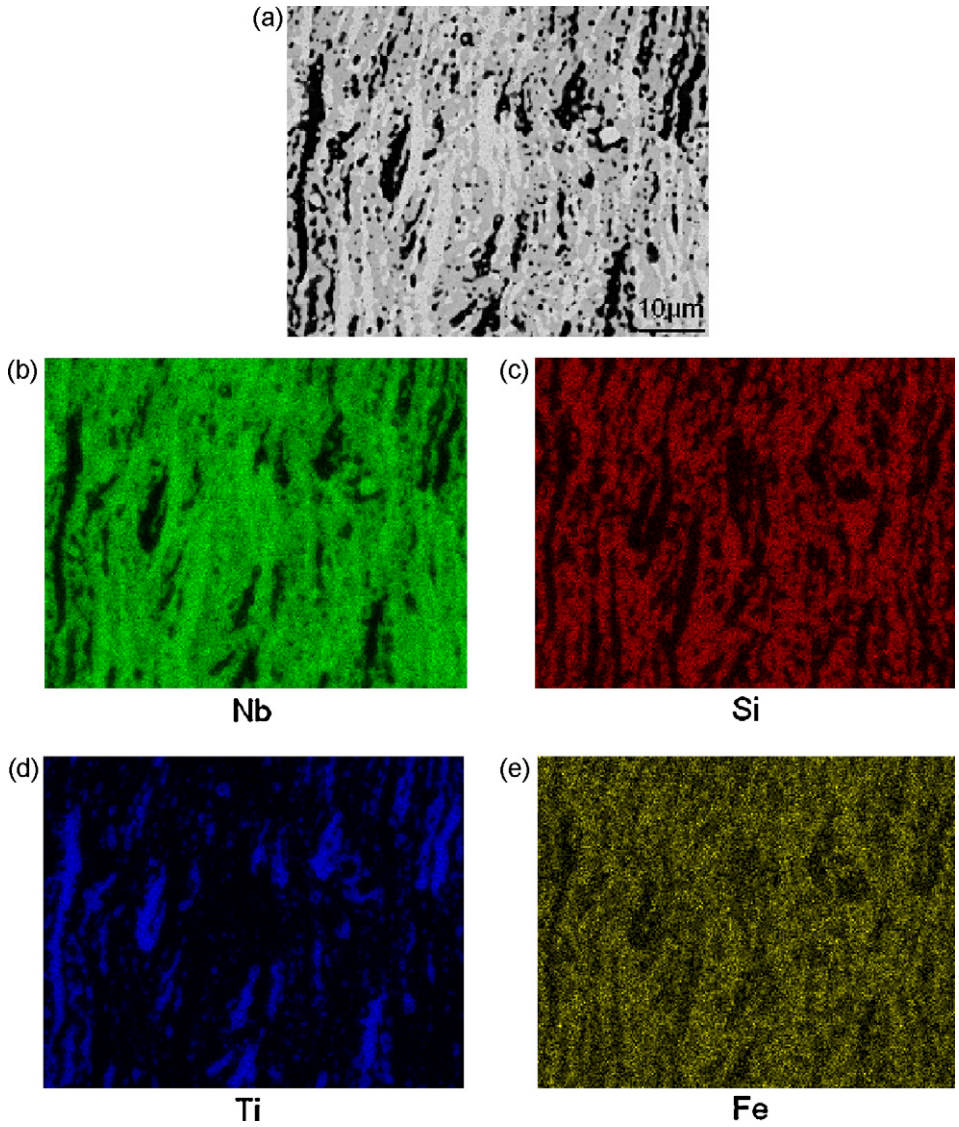

Fig. 7. EDX element mapping showing distribution of Nb (b), Si (c), Ti (d) and Fe (e) elements in the Nb–16Si–18Ti–3Fe alloy hot pressed from 30 h milled powders (a).

Table 2
Room temperature mechanical properties of the bulk alloys in this study.

Alloys	Flexural strength (MPa)	Fracture toughness ($MPa^{1/2}$)
Hot pressed from powders milled for 18 h		
Nb–16Si–Fe	394.05	8.9
Nb–16Si–3Fe	407.4	8.16
Nb–16Si–10Ti	570.75	14.64
Nb–16Si–10Ti–Fe	520.15	13.7 1
Nb–16Si–10Ti–3Fe	418.3	12.05
Nb–16Si–18Ti	660.4	16.3
Nb–16Si–18Ti–Fe	581.2	14.09
Nb–16Si–18Ti–3Fe	460.1	13.03
Hot pressed from powders milled for 30 h		
Nb–16Si–Fe	402.9	8.08
Nb–16Si–3Fe	414.97	7.31
Nb–16Si–10Ti	573.65	11.76
Nb–16Si–10Ti–Fe	519.9	11.08
Nb–16Si–10Ti–3Fe	422.35	9.61
Nb–16Si–18Ti	694.8	14
Nb–16Si–18Ti–Fe	586.7	12.34
Nb–16Si–18Ti–3Fe	508.95	10.08

ever, it was also observed that fracture toughness increased with the concentration of Fe decreasing, and hot-pressed alloys from powders mixtures milled for 18 h exhibited the distinctly higher fracture toughness than those consolidated from 30 h milled powders. In short, the fracture toughness ascended with the proportion of niobium solid solution increasing. Consequently, ductile-phase toughening was believed to be the crucial toughening mechanism in present work. Fig. 8 shows the crack propagation paths of hot-pressed Nb–16Si–18Ti–3Fe alloys after the three-point bending testes on the notched specimens. It can be seen that, besides the content of ductile Nb phase, its size also vitally influenced the fracture behavior of materials. It is obvious from Fig. 8 that crack bridging frequently occurred in the Nb–16Si–18Ti–3Fe alloy with larger size of ductile niobium phase, while crack deflection was often detected in that with smaller size of Nbss. A larger sized ductile particle can bear severe plastic deformation to trap the crack energy and provide the material with a higher toughness increment via a crack bridging mechanism. The toughening effect of an aligned eutectic microstructure was once evaluated according to the equation given by Ashby et al. [19]:

$$\Delta K_c = E\sqrt{CV_f\frac{\sigma_0}{E}a_0}$$

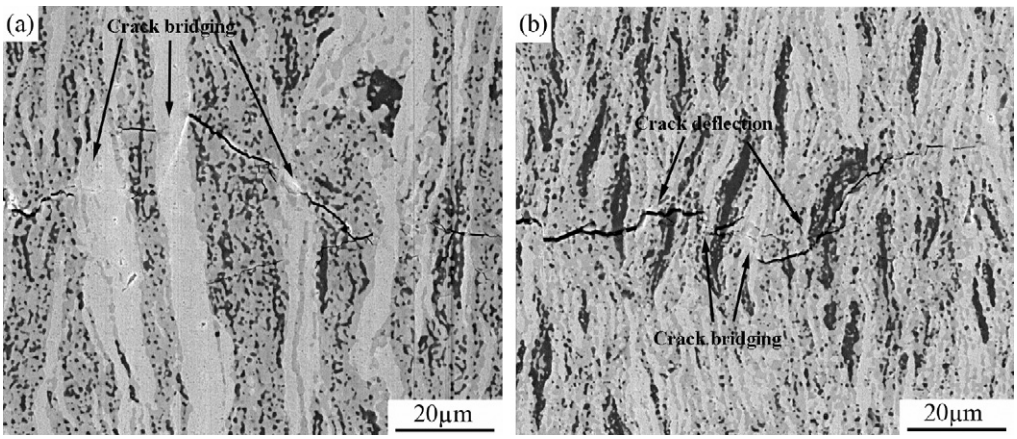

Fig. 8. Crack propagation behavior from fracture toughness tests on the notched Nb–16Si–18Ti–3Fe specimens consolidated from (a) 18 and (b) 30 h milled powders.

where ΔK_c is the toughness increment, E, V_f, σ_0, and a_0 are the Young's modulus, volume fraction, yield strength and radius of the ductile-phase particle, respectively. C is a material constant that represents the degree of constraint imposed upon a ductile particle from the matrix. Though it is difficult to do a quantitative analysis on the toughening effect of Nbss in this study, it can be concluded from the above equation that an increase in the size of Nbss contributed to the higher toughness. As a result, the fracture toughness of Nb–16Si–18Ti–3Fe alloy was enhanced by 29.3% from 10.08 to 13.03 $MPa^{1/2}$ when milling time decreased from 30 to 18 h.

Fig. 9 shows the fracture surfaces of Nb–16Si–3Fe and Nb–16Si–18Ti–3Fe alloys after three-point bending testes. River patterns were observed in the fractograph of Nb–16Si–3Fe alloy from 18 h milled powders, while the cleavage fracture surface of that from powders of 30 h milling was smooth. It suggests that the mobility of dislocation in lager sized Nbss was enhanced and fracture toughness was accordingly improved. However, Nb–16Si–18Ti–3Fe alloys displayed the widely different fractographs from those without titanium. The fracture surfaces of hot-pressed alloys with Ti were characterized by tear ridges that were clearer in the sample from powders of shorter milling time. It

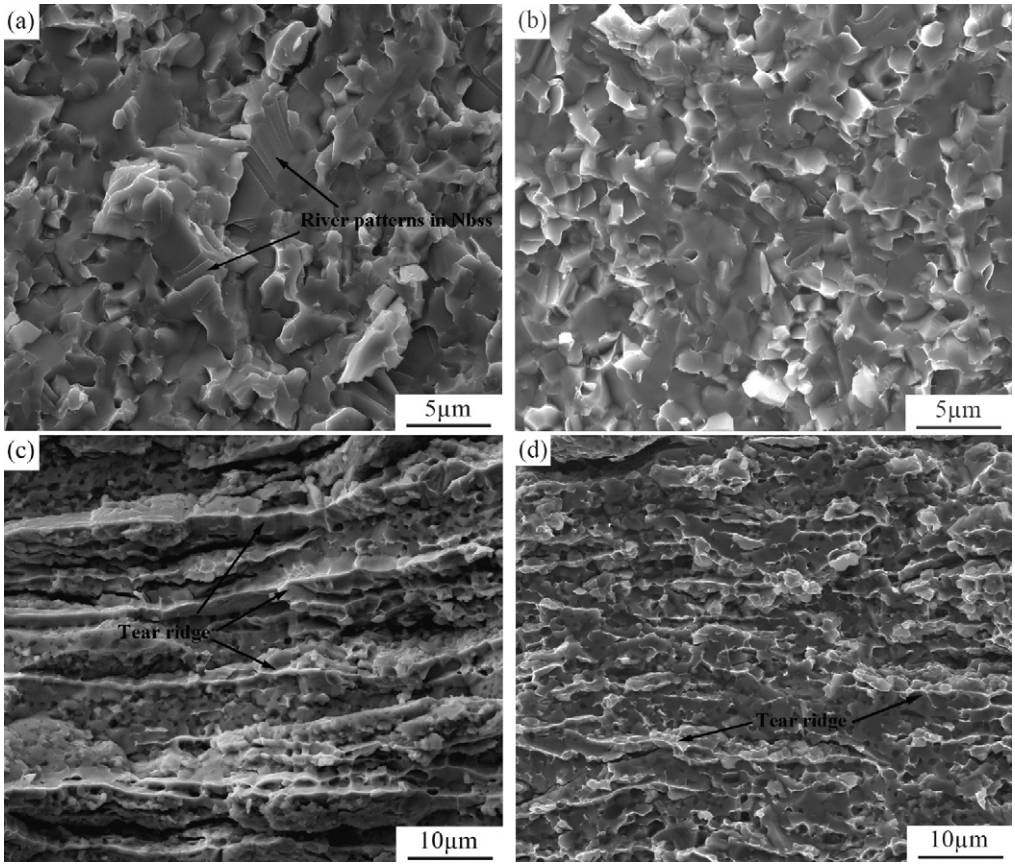

Fig. 9. Fractographs of three-point bending specimens: (a) and (b) for Nb–16Si–3Fe, (c) and (d) Nb–16Si–18Ti–3Fe; (a) and (c) are alloys from 18 h milled powders, while (b) and (d) are those from powder mixtures milled for 30 h.

indicates that, in the Ti-added alloys, Nb phase underwent significant plastic deformation and finally failed in a ductile manner.

4. Conclusions

Nb–Si alloys were fabricated by uniaxial hot pressing from ball milled Nb–Si–Ti–Fe powder mixtures with the fixed Si content (16 at.%) and various compositions of Ti and Fe, and the effects of Ti and/or Fe on the ball milling process, microstructure and room temperature mechanical properties of the materials were investigated. The conclusions of this works are as follows:

1. The addition of Ti in starting powder mixtures inhibits the ball milling process with the same milling parameters, and the refinement of Nb–16Si–18Ti–3Fe particles is much slower compared to Nb–16Si–3Fe powders. It is due to that, for the same weight, the powder mixtures containing Ti possess the higher volume since the lower density of Ti.
2. Nbss, Nb_3Si and Nb_5Si_3 are found in the hot-pressed alloys without Ti. Nbss, Tiss and Nb_5Si_3 phases are observed in the Ti-bearing alloys, while the expected Nb_3Si is not detected. It might be due to the lower composition of Ti in the reaction zone between the particles. In addition, Nb4FeSi is detected in the alloys with Fe, and the result of EDX elemental mapping shows iron mainly distributes in the niobium silicides. The Ti-added alloys hot pressed from a shorter time show the much coarser microstructure with Nbss in the shape of narrow strip distributed in river pattern, while near-equiaxed microstructure is obtained in the Nb–Si–Fe alloys. In the Ti-added alloys, both size and volume fraction of Nbss decrease with increasing milling time and Fe content. In addition, Fe mainly dissolves into niobium silicides and the solubility of Si in Nbss is improved with the addition of Ti. Besides, the concentration of Ti in Nbss increases with its content in the alloys increasing.
3. An enhancement in both room temperature fracture toughness and flexural strength is achieved in the alloys containing Ti. The fracture toughness decreases with increasing milling time for Ti-added alloys and Fe content for the alloys with fixed Ti content, because of the reduction in volume fraction of ductile Nbss phase. Besides, the large sized and banding Nbss in the alloys from a shorter milling time contribute to the crack bridging toughening and improve the toughness. However, the similar flexural strengths are detected in the alloys from 18 and 30 h milled powders. The flexural strength of the alloys from the shorter milling time is attributed to the solid solution strengthening, while the enhancement effect of reinforced phase contribute to the strength for the alloys from the longer milling time.

Acknowledgment

This work was supported by the National Natural Science Foundation of China (grant no. 50775052).

References

[1] C.L. Yeh, W.H. Chen, J. Alloys Compd. 425 (2006) 216.
[2] Z. Chen, Y.W. Yan, J. Alloys Compd. 413 (2006) 73.
[3] J. Geng, P. Tsakiropoulos, G. Shao, Intermetallics 15 (2007) 69.
[4] B.P. Bewlay, M.R. Jackson, J.C. Zhao, P.R. Subramanian, Metall. Mater. Trans. A 34 (2003) 2043.
[5] M.G. Mendiratta, J.J. Lewandowski, D.M. Dimiduk, Mettall. Trans. 22A (1991) 1573.
[6] W.Y. Kim, H. Tanaka, S. Hanada, Intermetallics 10 (2002) 625.
[7] L. Zhang, J. Wu, Acta Mater. 46 (1998) 3535.
[8] Y. Kimura, H. Yamaoka, N. Sekido, Y. Mishima, Mettall. Mater. Trans. A 36 (2005) 483.
[9] N. Sekido, Y. Kimura, S. Miura, F.G. Wei, Y. Mishima, J. Alloys Compd. 425 (2006) 223.
[10] B.P. Bewlay, M.R. Jackson, P.R. Subramanian, JOM 51 (1999) 32.
[11] K.S. Chan, D.L. Davidson, Mettall. Mater. Trans. A 32 (2001) 2717.
[12] R.O. Ritchie, Mater. Sci. Eng. A 103 (1988) 15.
[13] A.G. Evans, J. Am. Ceram. Soc. 73 (1990) 187.
[14] N. Sekido, Y. Kimura, F.G. Wei, S. Miura, Y. Mishima, J. Jpn. Inst. Met. 64 (2000) 1056.
[15] N. Sekido, Y. Kimura, S. Miura, Y. Mishima, Mater. Trans. 45 (2004) 3264.
[16] W.O. Soboyejo, F. Ye, L.C. Chen, N. Bahtishi, D.S. Schwartz, R.J. Lederich, Acta Mater. 44 (1996) 2027.
[17] X. Sun, J.A. Yeomans, J. Mater. Sci. 31 (1996) 875.
[18] D.R. Bloyer, K.T.V. Rao, R.O. Ritchie, Metall. Mater. Trans. 29A (1998) 2483.
[19] M.F. Ashby, F.J. Blunt, M. Bannister, Acta Metall. 37 (1989) 1847.
[20] B.P. Bewlay, M.R. Jackson, W.J. Reeder, H.A. Lipsitt, Mater. Res. Soc. Symp. Proc. 364 (1995) 943.
[21] P.R. Subramanian, M.G. Mendiratta, D.M. Dimiduk, M.A. Stucke, Mater. Sci. Eng. A 239–240 (1997) 1.
[22] J. Geng, P. Tsakiropoulos, G. Shao, Intermetallics 14 (2006) 227.
[23] K. Zelenitsas, P. Tsakiropoulos, Intermetallics 13 (2005) 1079.
[24] N. Vellios, P. Tsakiropoulos, Intermetallics 15 (2007) 1529.
[25] B.P. Bewlay, M.R. Jackson, J. Phase Equilib. 19 (1998) 577.
[26] Z. Li, L.M. Peng, Acta Mater. 55 (2007) 6573.
[27] J.L. Yu, K.F. Zhang, Z.K. Li, X. Zheng, G.F. Wang, R. Bai, Scripta Mater. 61 (2009) 620.
[28] H. Liang, Y.A. Chang, Intermetallics 7 (1999) 561.
[29] J.B. Sha, H. Hirai, T. Tabalu, A. Kitahara, H. Ueno, S. Handa, Metall. Mater. Trans. 43A (2003) 2861.
[30] K.S. Chan, Mater. Sci. Eng. A 329–331 (2002) 513.
[31] K.S. Chan, Mater. Sci. Eng. A 409 (2005) 257.